FINITE-VOLUME SOLUTION OF A CYLINDER IN CROSS FLOW WITH HEAT TRANSFER

B. Mirzaee and E. Khoshravan

Department of Mechanical Engineering, University of Tabriz
Tabriz, Iran, ekhosh@ark-tabrizu-ac.ir

S. E. Razavi

Department of Mechanical Engineering, Sahand University of Technology
Tabriz, Iran

Abstract   A finite-volume model has been developed to study incompressible forced flow heat transfer of air over a circular cylinder in cross flow. An artificial compressibility technique is applied to couple the continuity to the momentum equations. The proposed explicit finite-volume method (FVM) uses a novel discretization in time and space. The governing equations are solved by time-marching using a new third- order algorithm at each time level. The discretization of the viscous and thermal conduction terms are very simplified using the new scheme instead of common methods. The new scheme is similar to the Jameson's flux averaging in the convective terms, while for viscous and thermal conduction terms, the first- order derivatives are averaged in the vicinity of two cells. The proposed model is able to converge at higher Reynolds numbers up to 101000. The numerical results agree well with the available experimental and numerical data. The proposed FVM is capable of capturing the flow details at wide range of Reynolds numbers.

چکیده   مدلی بر اساس روش حجم محدود برای مطالعه جریان صلیبی سیال غیر قابل تراکم و همراه با انتقال حــرارت از روی استوانه توسعه داده شده است. برای پیوند معادلات پیوستگی و ممنتوم ، تکنیک ضریب تراکم پذیــری مصــنوعی اعمــال شــده است. در روش حجم محدود پیشنهادی و صریح، برای گسسته سازی مشتقات زمانی و مکانی طرحهای جدیدی بکار رفته اند. جملات زمانی معادلات حاکمه با طرح جدید از مرتبه سوم و با الگــوی زمانروی حل می‌شوند. در گسسته سازی جملات لزجت و رسانش سیال، با استفاده از یک طرح جدید بــه جــای طــرحهای مرسوم، ساده سازی قابل ملاحظه ای صورت گرفته است. این طرح شبیه به طرح اختلاف مرکــزی در گسســته ســازی عــبارتهای همرفت است، با این تفاوت که در مرز دو سلول مجاور بجای میانگیری متغیرهای وابسته، از میانگین مشتق اول آنها استفاده می‌شود. مدل پیشنهادی قادر است برای اعداد رینولدز بالا و تــا ۱۰۱۰۰۰ همگــرا شود. نتایج حاصله تطابق خوبی با نتایج موجود تجربی و عددی دارد. روش حجم محدود پیشنهادی توانائی آشکار نمودن رفتارهای جزئی سیال در محدوده وسیعی از اعداد رینولدز را داراست.

1. INTRODUCTION

Many forms of heat exchangers are employed in the different branches of modem technology. Curvilinear bodies in cross flow constitute a very common group of elements in such devices. These may be circular cylinders, rectangular or elliptic pipes, and bodies of other geometries. Circular cylinders find perhaps the most widespread application in heat exchangers, power generators, and other thermal apparatus. The circular cylinder constitutes a classical element in boilers, steam or gas turbines, compressors, and in various aerodynamic problems. A variety of cross-sections are also used in buildings, chimneys, etc.

With a cylinder in laminar cross-flow, boundary layer is formed on the front part as a result of viscous forces. It is commonly accepted that, in the lower range of Reynolds number ($Re \cong 1$), the cylinder is enveloped all around by a laminar boundary layer, which separates from its surface only at the rear stagnation point. An increase of

Re leads to an increase in the effect of inertial forces, so that the laminar boundary layer separates from the surface at the certain distance from the rear stagnation point, and a complex vortex structure is formed in the wake (Re<2.10^5) [1]. For Reynolds numbers less than 40 the separated flow is steady. In the range of Reynolds numbers from about 60 to about 5000 there exists behind the cylinder a Karman vortex street which shows a regular, periodic structure [2]. The heat transfer in the rear part is governed by a vortex-separated flow. An interpretation in terms of Nu = c.Re^m.Pr^n was a long time commonly accepted for experimental data on heat transfer [l].

Numerical methods have been used by a number of investigators to deal with the problem of fluid flow and heat transfer over a circular cylinder. An efficient code is the key to solution methodologies which would produce results using the least amount of computing time and memories. This is particularly true for problems with high Reynolds numbers. Most of the previous numerical studies have been done for Reynolds numbers less than 5000. Krall and Eckert [3] studied forced convection for Reynolds numbers up to 200 using the donor-cell technique. Chun and Boehm [4] carried out an analysis for Reynolds numbers up to 3480 by stream function-vorticity approach along with a mapping transformation. Also they assumed the line symmetry in treating the wake region, which is not physically meaningful. The vorticity-stream function loses its capability when applied to three-dimensional flows because stream function does not exist in this case [5]. Most of the previous studies have used the central difference scheme [3,4].

Algorithms for solving the Euler and Navier-Stokes equations with FVMs have been grown in recent years [6,7,8,9]. The FVM of Jameson et al has proved to be useful as a tool for aerodynamic applications and even in solving the Navier-stokes equations [9,10,11,12]. Among the various schemes proposed for the flux calculation in FVMs [13,14], the Jameson's flux averaging is still of use because of its simplicity. In FVM a mapping is not needed. Therefore the scheme is applied directly in the physical domain.

Lin and Wu [15] presented an algorithm for solving the two-dimensional incompressible Navier-Stokes equations. They applied an artificial

compressibility method using higher-order upwind FVM for the convective terms and a second-order scheme for the viscous terms at Reynolds numbers of 20 and 40.

To suppress the tendency for odd and even point decoupling, in the central differencing schemes are added the artificial dissipation terms [6,16]. The artificial dissipation is not needed in the proposed method.

In this paper, a new third-order algorithm is devised for time discretization instead of the fourth-order Runge-Kutta scheme. The new third-order algorithm resulted in the rapid convergence in comparison to the fourth-order Runge-Kutta scheme [17]. Also the rate of convergence of the proposed FVM has proved to be faster than the other time discretization methods [17]. The artificial compressibility approach is applied, which produces a hyperbolic-dominated system of equations. An advantage of the proposed algorithm is that it can solve the flow around cylinder at quite high Reynolds numbers up to 200,000.

2. GOVERNING EQUATIONS

The integral form of the Navier-Stokes equations with artificial compressibility can be written as:

$$\frac{\partial}{\partial t}\iint_{\partial A} Q d\Omega + \oint_{\partial A}(Fdy - Gdx) = \oint_{\partial A}(Rdy - Sdx) \quad (1)$$

$$Q = \begin{bmatrix} p \\ u \\ v \\ \theta \end{bmatrix}, F = \begin{bmatrix} \beta u \\ u^2 + p \\ uv \\ u\theta \end{bmatrix}, G = \begin{bmatrix} \beta v \\ uv \\ v^2 + p \\ v\theta \end{bmatrix},$$

$$R = \frac{1}{Re}\begin{bmatrix} o \\ \dfrac{\partial u}{\partial x} \\ \dfrac{\partial v}{\partial x} \\ \dfrac{1}{Pr}\dfrac{\partial\theta}{\partial x} \end{bmatrix}, S = \frac{1}{Re}\begin{bmatrix} o \\ \dfrac{\partial u}{\partial y} \\ \dfrac{\partial v}{\partial y} \\ \dfrac{1}{Pr}\dfrac{\partial\theta}{\partial y} \end{bmatrix}$$

(2)

in which A and ∂ A are the domain area and perimeter

respectively. The vector Q shows the pressure, the Cartesian velocity components and the temperature. The artificial compressibility parameter is denoted by β and Re is the diameter based Reynolds number. Pr shows the Prandtl number. The Prandtl number is assumed to be constant and for air Pr=0.7 is considered. Equation 1 is in non-dimensional form by applying the following relations:

$$x^* = \frac{x}{D}, y^* = \frac{y}{D}, u^* = \frac{u}{u_\infty}, v^* = \frac{v}{u_\infty}$$

$$t^* = \frac{t}{D/u_\infty}, p^* = \frac{p - p_\infty}{\rho u_\infty^2}, \mathrm{Re} = \frac{u_\infty D}{v}, \mathrm{Pr} = \frac{\alpha}{v}$$

(3)

$$\theta^* = \frac{T - T_\infty}{T_w - T_\infty} \quad \text{uniform wall temperature(UWT)}$$

(4)

For simplicity the * has been eliminated in Equation 1. After some algebraic manipulations, Equation 1 can be written as:

$$\frac{dp}{dt} = \frac{1}{A} f_1(\beta, x, y, u, v)$$ (5-a)

$$\frac{du}{dt} = \frac{1}{A} f_2(x, y, p, u, v, \mathrm{Re})$$ (5-b)

$$\frac{dv}{dt} = \frac{1}{A} f_3(x, y, p, u, v, \mathrm{Re})$$ (5-c)

$$\frac{d\theta}{dt} = \frac{1}{A} f_4(x, y, u, v, \theta, \mathrm{Re}, \mathrm{Pr})$$ (5-d)

in which p, u, v and θ are the pressure, the Cartesian velocity and the temperature, stored in the cell centers. A denotes the cell area. Equations 5 show that the governing equations are the first order ordinary differential equations with respect to time.

3. GRID FEATURES

Grid is generated algebraically where the clustering was used near the cylinder surface (Figure 1). The following hyperbolic function was used for clustering the cells in the vicinity of the cylinder
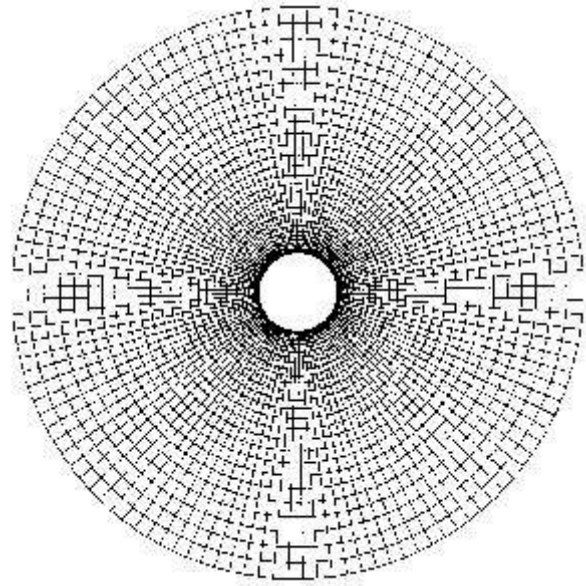

Figure 1. A part of 120x120 algebraic grid for the circular cylinder.

surface:

$$g = \frac{\tanh(B \frac{j-1}{JM})}{\tanh(B)}, B = \frac{1}{2}\ln(\frac{\eta-1}{\eta+1}) \quad , \eta > 1$$ (6)

As the η approaches unity, more grid points are clustered near the solid wall. In this work a 120x120 grid were used, with circular far-field having the semi axes at 30 chords. It should be noted that, in Figure 1 only a part of the 120x 120 grid is shown.

4. BOUNDARY CONDITIONS

Good solid boundary conditions must ensure the disturbance dissipation in the discretized domain without reflection [10,16]. On the solid boundary, the usual no-slip condition is applied, $\theta = 1$. u=0, v=0 and the pressure at the wall is obtained by setting the normal gradient of p equal to zero at the no-slip wall, $i.e. \partial p / \partial n = 0$[15] .For the energy equation, the boundary condition is $\theta = 1$ at solid boundary[4].

At the far-field boundary, characteristic boundary conditions are used. The inflow boundary condition is computed by two free stream and one extrapolated from the interior. This can be written

in terms of the left eigenvector L as [15]:

$$
\begin{pmatrix} l_{11} & l_{12} & l_{13} \\ l_{21} & l_{22} & l_{23} \\ l_{31} & l_{32} & l_{33} \end{pmatrix} \begin{pmatrix} p \\ u \\ v \end{pmatrix}_{boundary} = \begin{pmatrix} (l_{11}p + l_{12}u + l_{13}v)_{freestream} \\ (l_{21}p + l_{22}u + l_{23}v)_{freestream} \\ (l_{31}p + l_{32}u + l_{33}v)_{int\,rerior} \end{pmatrix}
$$

(7)

For the outflow boundary, only one boundary condition can be imposed [15].

$$
\begin{pmatrix} l_{11} & l_{12} & l_{13} \\ l_{21} & l_{22} & l_{23} \\ l_{31} & l_{32} & l_{33} \end{pmatrix} \begin{pmatrix} p \\ u \\ v \end{pmatrix}_{boundary} = \begin{pmatrix} (l_{11}p + l_{12}u + l_{13}v)_{freestream} \\ (l_{21}p + l_{22}u + l_{23}v)_{intrerior} \\ (l_{31}p + l_{32}u + l_{33}v)_{intrerior} \end{pmatrix}
$$

(8)

For the energy equation, the boundary condition $\theta = 0$ is used at far-field [4].

5. DISCERTIZATION OF THE GOVERNING EQUATIONS

5.1 Time Discretization For numerical solution of the first-order ordinary differential Equations 5, a new third-order algorithm has been proposed by Mirzaee, instead of the classical fourth-order Runge-Kutta scheme [17]. To describe briefly, Equation 5-b is integrated from time level n to time level n+1/2 and also n+l (Figure 2). Therefore one can write:

$$
u_{i,j}^{n+\frac{1}{2}} = u_{i,j}^n + \frac{1}{A} \int_0^{\Delta t/2} f_2(x, y, p, u, v, \mathrm{Re})dt
$$

$$
u_{i,j}^{n+1} = u_{i,j}^n + \frac{1}{A} \int_0^{\Delta t} f_2(x, y, p, u, v, \mathrm{Re})dt
$$

(9)

In which Δt is the time step and $u_{i,j}^{n+1/2}$ and $u_{i,j}^{n+1}$ are the values of $u_{i,j}$ in the time levels n+1/2 and n+1, respectively. Then $\overline{(du/dt)}_{i,j}^{n+1/2}$ and $\overline{(du/dt)}_{i,j}^{n+1}$ are defined such as the mean values of the first-order time derivatives in the time intervals [0, Δt/2] and [0,Δt], respectively.
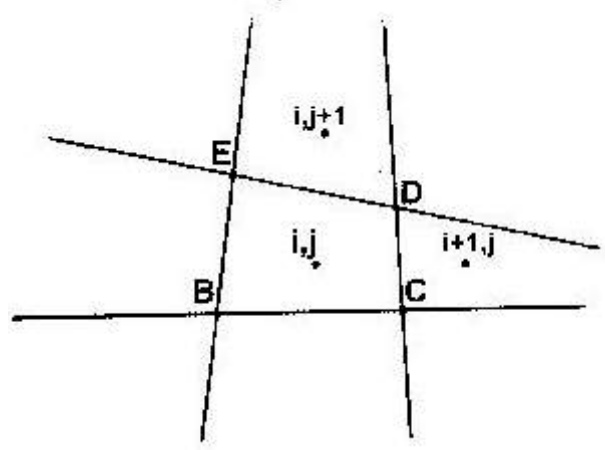
Therefore one has:

Figure 2. Cells in the finite- volume approach.

$$
\left(\overline{\frac{du}{dt}}\right)_{i,j}^{n+\frac{1}{2}} = \frac{1}{\Delta t/2} \int_0^{\Delta t/2} f_2(x, y, p, u, c, \mathrm{Re})dt
$$

$$
\left(\overline{\frac{du}{dt}}\right)_{i,j}^{n+1} = \frac{1}{\Delta t} \int_0^{\Delta t} f_2(x, y, p, u, c, \mathrm{Re})dt
$$

(10)

Then the following relations are resulted:

$$
u_{i,j}^{n+\frac{1}{2}} = u_{i,j}^n + \frac{\Delta t/2}{A}\left(\overline{\frac{du}{dt}}\right)_{i,j}^{n+\frac{1}{2}}
$$

$$
u_{i,j}^{n+1} = u_{i,j}^n + \frac{\Delta t}{A}\left(\overline{\frac{du}{dt}}\right)_{i,j}^{n+1}
$$

(11)

$\overline{(du/dt)}_{i,j}^{n+1/2}$ and $\overline{(du/dt)}_{i,j}^{n+1}$ are corrected by the following equations[17]:

$$
\left(\overline{\frac{du}{dt}}\right)_{i,j}^{n+\frac{1}{2}} = \frac{5}{12}\left(\overline{\frac{du}{dt}}\right)_{i,j}^n + \frac{2}{3}\left(\overline{\frac{du}{dt}}\right)_{i,j}^{n+\frac{1}{2}} - \frac{1}{12}\left(\overline{\frac{du}{dt}}\right)_{i,j}^{n+1}
$$

$$
\left(\overline{\frac{du}{dt}}\right)_{i,j}^{n+1} = \frac{1}{6}\left(\overline{\frac{du}{dt}}\right)_{i,j}^n + \frac{2}{3}\left(\overline{\frac{du}{dt}}\right)_{i,j}^{n+\frac{1}{2}} + \frac{1}{6}\left(\overline{\frac{du}{dt}}\right)_{i,j}^{n+1}
$$

(12)

in which $(du/dt)_{i,j}^{n}$, $(du/dt)_{i,j}^{n+1/2}$ and $(du/dt)_{i,j}^{n+1}$ are the first-order time derivatives of $u_{i,j}$ in the time level n, n+1/2 and n+l, respectively. $(du/dt)_{i,j}^{n+1/2}$ and $(du/dt)_{i,j}^{n+1}$ are obtained from substituting Equation 11 into Equation 5-b. In the third-order Mirzaee algorithm, one can observe that the procedure for solving $u_{i,j}^{n+1}$ is necessarily an iterative process at each time level. Beginning at the time level n, $\overline{(du/dt)}_{i,j}^{n+1/2}$ and $\overline{(du/dt)}_{i,j}^{n+1}$ are taken the values of $(du/dt)_{i,j}^{n}$, and then corrected by Equation 12. The process is repeated until $u_{i,j}^{n+1}$ converges to a certain value.

5.2 Space Discretization

Right hand side of Eqs. (5) is written at time level n as:

$$\frac{dp}{dt} = \frac{1}{A} \oint_{\partial A} \beta(vdx - udy)$$

$$\frac{du}{dt} = \frac{1}{A} \left\{ \frac{1}{Re} \oint_{\partial A} [\frac{\partial u}{\partial x} dy - \frac{\partial u}{\partial y} dx] - \oint_{\partial A} [(u^2 + p)dy - (uv)dx] \right\}$$

$$\frac{dv}{dt} = \frac{1}{A} \left\{ \frac{1}{Re} \oint_{\partial A} [\frac{\partial v}{\partial x} dy - \frac{\partial v}{\partial y} dx] - \oint_{\partial A} [(uv)dy - (v^2 + p)dx] \right\}$$

(13)

also one has:

$$\frac{d\theta}{dt} = \frac{1}{A} \left\{ \frac{1}{Re\,Pr} \oint_{\partial A} [\frac{\partial \theta}{\partial x} dy - \frac{\partial \theta}{\partial y} dx] - \oint_{\partial A} [(u\theta)dy - (v\theta)dx] \right\}$$

(14)

Equations 13 and 14 show that the viscous and thermal conduction terms have similar form, so they can be discretized in the same way. System of ordinary differential equations is obtained by applying Equations 13 and 14 to each cell separately. For example in Equation 14 for the convective term, we choose the flux-averaging scheme. In this scheme each quantity such as $(u\theta)_{CD}$ and $(v\theta)_{CD}$ is evaluated as the average of the cells on either side of the face (Figure 2):

$$(u\theta)_{CD} = \frac{1}{2}[(u\theta)_{i,j} + (u\theta)_{i+1,j}]$$

$$(v\theta)_{CD} = \frac{1}{2}[(v\theta)_{i,j} + (v\theta)_{i+1,j}]$$

(15)

Flux averaging is applied here for the viscous and thermal conduction terms. In this new method, we need to know the first-order derivatives such as $(\partial\theta/\partial x)_{i,j}$ and $(\partial\theta/\partial y)_{i,j}$ and so on (at the cell centre). To calculate the unknowns such as $(\partial\theta/\partial x)_{i,j}$ and $(\partial\theta/\partial y)_{i,j}$, The Taylor series are used. As seen in Figure 2, for variables of the cell vertices, such as θ_B one has:

$$\theta_B = \frac{1}{4}(\theta_{i,j} + \theta_{i,j-1} + \theta_{i-1,j-1} + \theta_{i-1,j})$$

(16)

Therefore the information of the fourth points such as B, C, D and E are found. To find the values of $(\partial\theta/\partial x)_{i,j}$ and $(\partial\theta/\partial y)_{i,j}$, one should use the Taylor series as:

$$\begin{bmatrix} x_B - x_{i,j} & y_B - y_{i,j} & \frac{(x_B-x_{i,j})^2}{2} & \frac{(y_B-y_{i,j})^2}{2} \\ x_C - x_{i,j} & y_C - y_{i,j} & \frac{(x_C-x_{i,j})^2}{2} & \frac{(y_C-y_{i,j})^2}{2} \\ x_D - x_{i,j} & y_D - y_{i,j} & \frac{(x_D-x_{i,j})^2}{2} & \frac{(y_D-y_{i,j})^2}{2} \\ x_E - x_{i,j} & y_E - y_{i,j} & \frac{(x_E-x_{i,j})^2}{2} & \frac{(y_E-y_{i,j})^2}{2} \end{bmatrix} \times \begin{bmatrix} \left(\frac{\partial\theta}{\partial x}\right)_{i,j} \\ \left(\frac{\partial\theta}{\partial y}\right)_{i,j} \\ \left(\frac{\partial^2\theta}{\partial x^2}\right)_{i,j} \\ \left(\frac{\partial^2\theta}{\partial y^2}\right)_{i,j} \end{bmatrix} = \begin{bmatrix} \theta_B - \theta_{i,j} \\ \theta_C - \theta_{i,j} \\ \theta_D - \theta_{i,j} \\ \theta_E - \theta_{i,j} \end{bmatrix}$$

(17)

For the first thermal conduction term in Equation 14, we use the central differencing scheme. Each quantity for example $(\partial\theta/\partial x)_{CD}$ and $(\partial\theta/\partial y)_{CD}$ is found such as:

$$\left(\frac{\partial\theta}{\partial x}\right)_{CD} = \frac{1}{2}\left[\left(\frac{\partial\theta}{\partial x}\right)_{i,j} + \left(\frac{\partial\theta}{\partial x}\right)_{i+1,j}\right]$$

$$\left(\frac{\partial\theta}{\partial y}\right)_{CD} = \frac{1}{2}\left[\left(\frac{\partial\theta}{\partial y}\right)_{i,j} + \left(\frac{\partial\theta}{\partial y}\right)_{i+1,j}\right]$$

(18)

6. NUMERICAL RESULTS

To investigate the performance of the proposed

FVM, a series of tests were conducted. Error norm is defined by:

$$Error = \frac{\sum_{i=1}^{IM} \sum_{j=1}^{JM} \sqrt{(u_{i,j}^{n+1} - u_{i,j}^{n})^2}}{IM \times JM} \qquad (19)$$

where IM and JM are the cell numbers along circumferential and radial directions respectively. In this work the convergence criteria was set to 10^{-7}.

In Figure 3 the angular distribution of local Nusselt number along the circumference of the cylinder for different values of β are plotted at Re=50. Results show that the solutions are not sensitive to β. In Figure 4 the total drag C_D is plotted versus Reynolds number and is compared with the numerical solutions of the other investigator [1]. The C_D includes both skin drag and pressure drag. Figure 4 illustrates that as the Reynolds number increases, the viscous effects become restricted more and more to the boundary layer and there is a decreasing C_D. After Re = 5000, is shown the considerable rise in the C_D. This is due to the separation process moving toward the top and bottom of the cylinder. When separation occurs closer to the top and bottom of the cylinder with little pressure recovery in the wake, there is a smaller pressure in the back of cylinder, thus resulting in greater drag.

Figure 5 represent streamlines for the selected Reynolds numbers. As is shown, the recirculation zone or wake is generated behind a cylinder. Also these plots show that, the wake affects the path line and acts like "aerodynamic rollers" over which the main stream flows.

Isotherms are plotted in Figure 6 and Figure 7. We know that the temperature gradient causes these phenomena. As is shown, isotherms are restricted to the boundary layer and those effects are seen in the wake. Also the temperature contours do not show any symmetry.

Local Nusselt numbers for a circular cylinder in cross flow are plotted in Figure 8 and are compared with the numerical solutions of the other investigators [4]. The present numerical results agree well with them. These plots show the angular distribution of local Nu along the circumference of
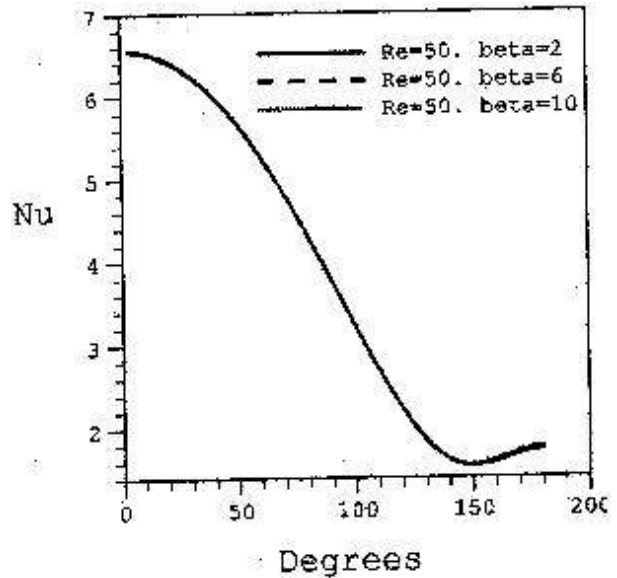

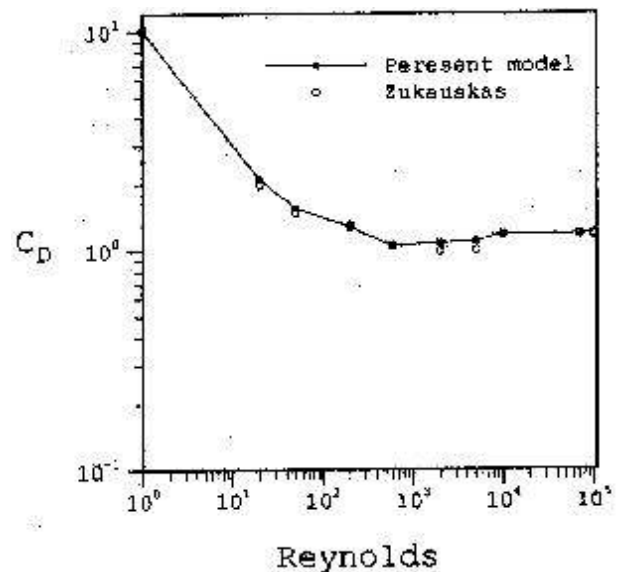**Figure 3**. Independency of Nu to β.

Figure 4. Comparison of total drag for different Reynolds numbers, with the experimental results of [1].

cylinder in which the peak at the front stagnation point is observed. This is anticipated, since the downstream growth of a thermal boundary layer would certainly increase the thermal resistance.
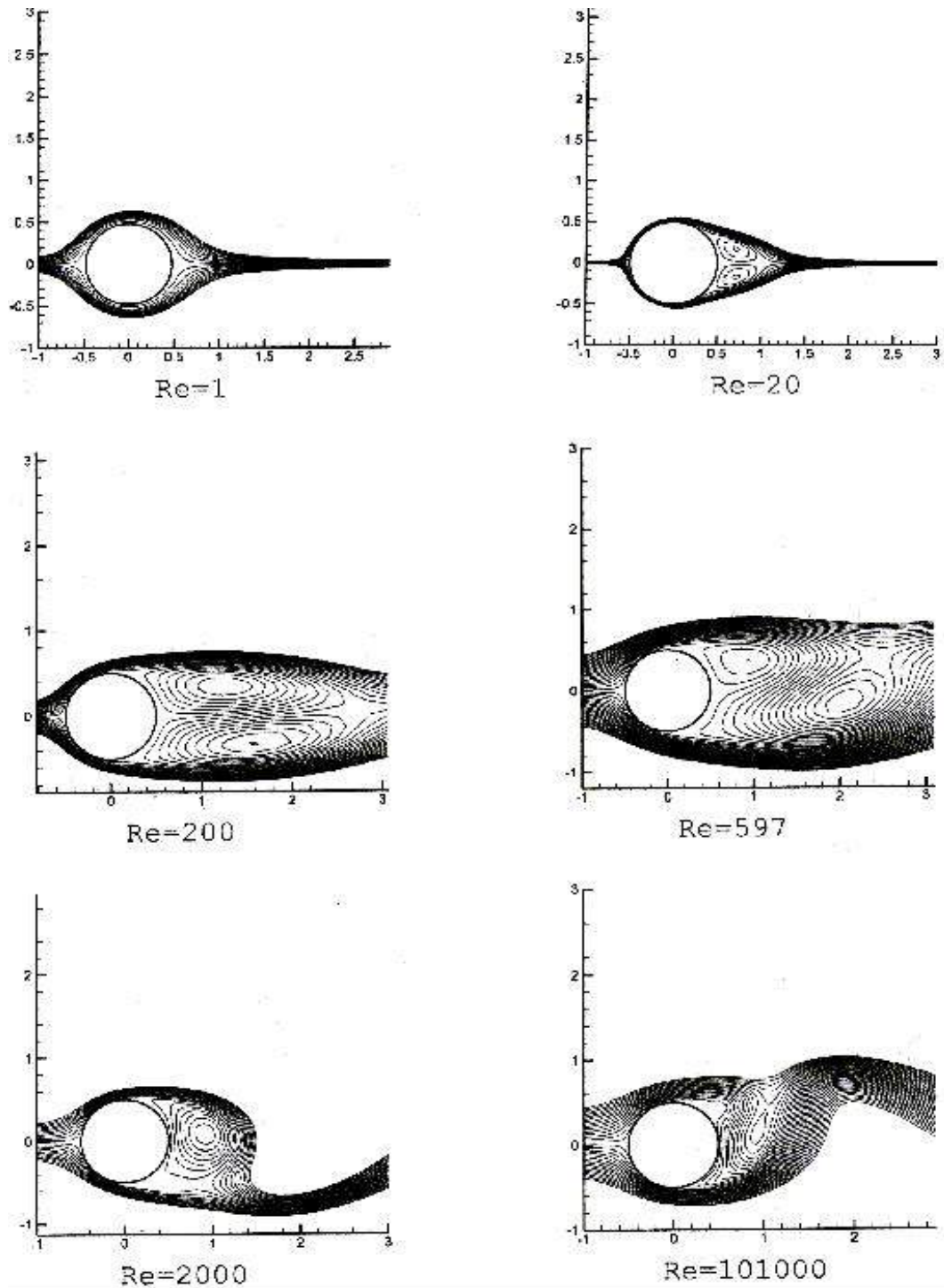
Figure 5. Streamlines of 2D flow over a circular cylinder for different Reynolds numbers.

In Figure 9 local Nusselt numbers are plotted at Re=71000 and Re=101000, and are compared with the experimental data [I8], Also in Figure 10 is plotted the convergence history versus the iteration
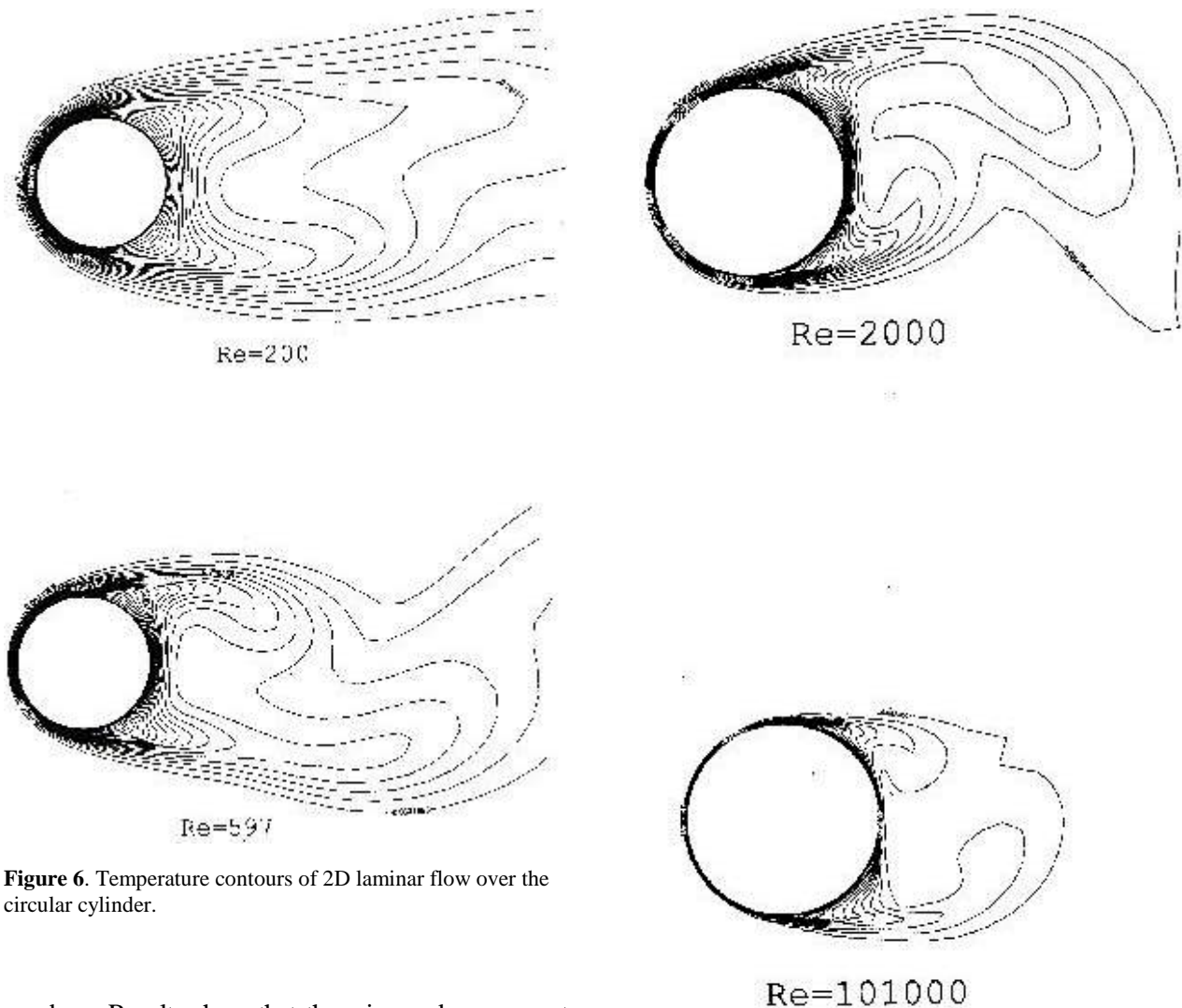
Figure 6. Temperature contours of 2D laminar flow over the circular cylinder.

numbers. Results show that there is good agreement with the Giedt.

In Figures 11a and 11b the peak values of the local Nu at the front stagnation point for different Reynolds numbers, are plotted and compared with the experimental formula of Sarma and Sukhatme $Nu_{sp}=0.91\,Re^{0.5}$ [4]. An acceptable agreement does exist.

Figure 12a shows the calculated average Nuselt numbers up to Re=597 for the UWT case. In this figure the numerical solutions of other investigators are compared with the present results and good agreement would exist.

Figure 12b shows the calculated average Nusselt numbers up to Re=10,000, for the UWT case. Herein, the present results are compared with the two different proposed experimental formulas. One of them is the experimental formula of Zukauskas [18]:

Figure 7. Temperature contours of 2D laminar flow over the circular cylinder.

$$\overline{Nu} = c\,Re^{m}\,Pr^{n}$$
$$c = 0.51, m = 0.5\ when\quad 40 < Re < 1000$$
$$c = 0.26, m = 0.6\ when\quad 1000 < Re < 200000$$

$$(20)$$

And other is the experimental formula of Churchill and Bernstein[18]:

$$\overline{Nu} = 0.3 + \frac{0.62\,Re^{1/2}\,Pr^{1/3}}{[1+(0.4/Pr)^{1/3}]^{1/4}}\left[1+\left(\frac{Re}{282000}\right)^{5/8}\right]^{4/5}$$
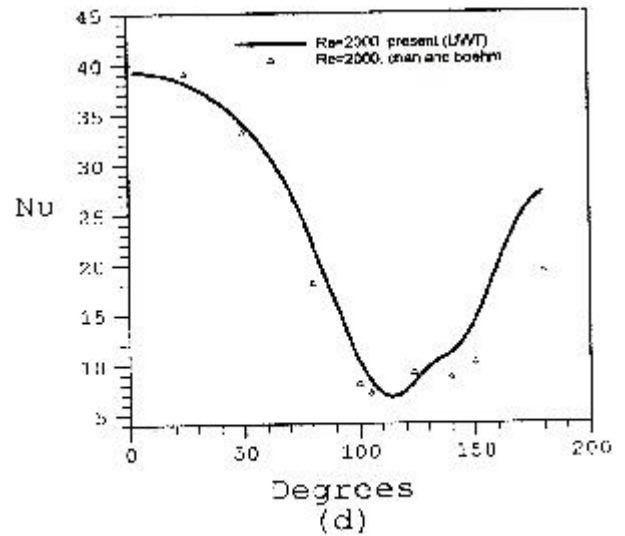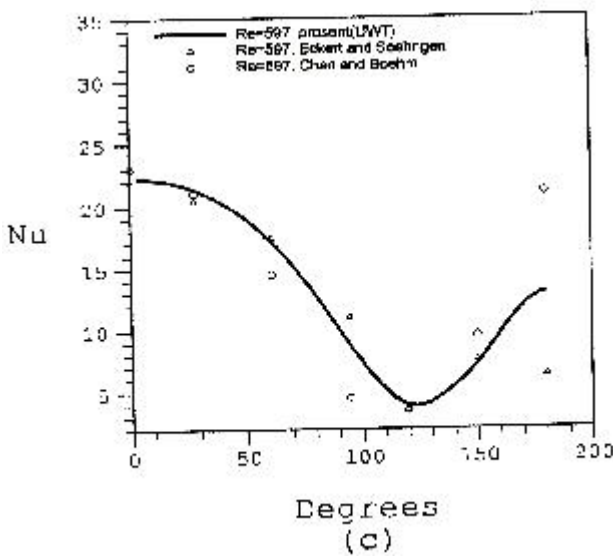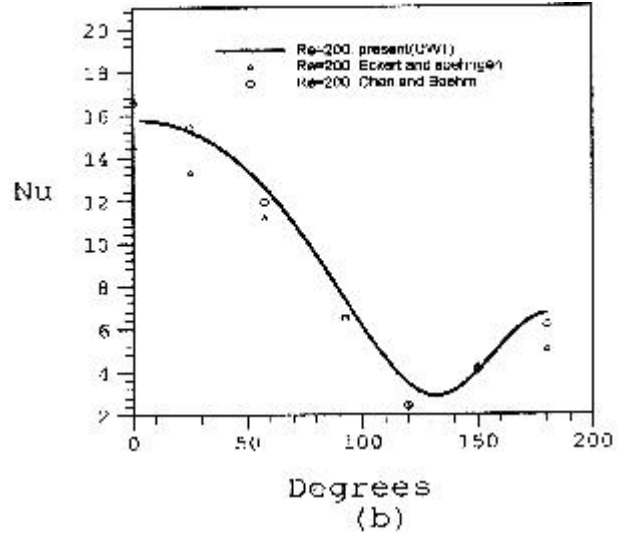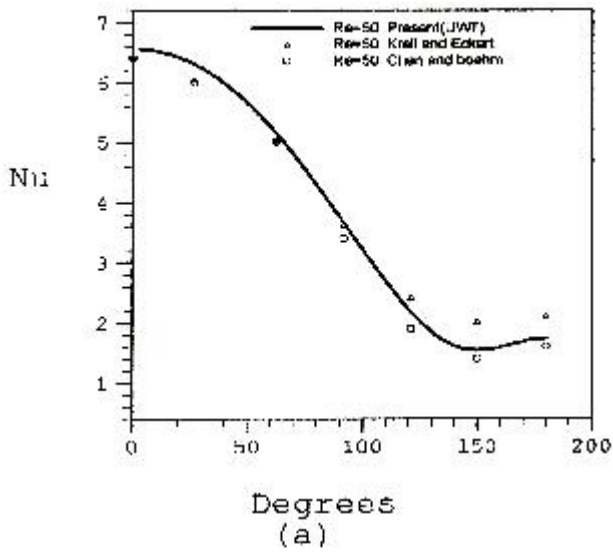$$, Re\,Pr > 0.2$$

$$(21)$$

Figure 8. Comparison of the local Nu of FVM with other investigaters.

As it is seen, from Figure 12b, close agreement dose exist between the results of the proposed FVM and the experimental formulas.

7. CONCLUDING REMARKS

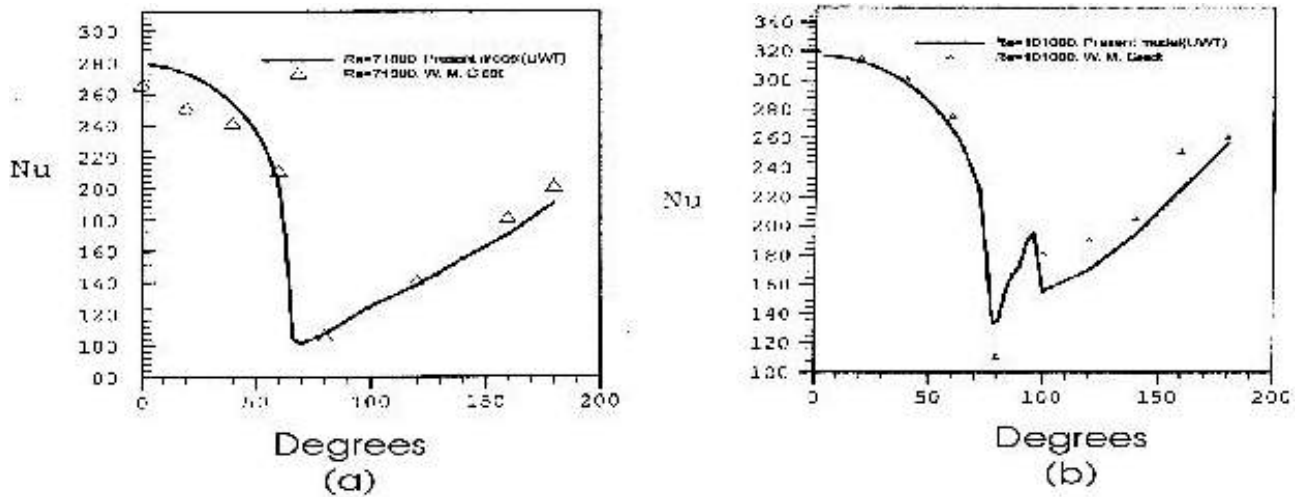The novel FVM developed in the present work was

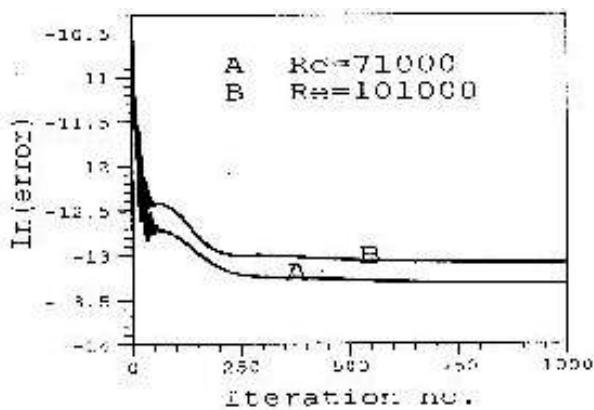**Figure 9**. Comparison of the local Nu of FVM with other investigator.

Figure 10. Comparison of convergence histories at different Reynolds numbers.

quite successful in predicting the forced flow heat transfer of air over a circular cylinder in cross flow. This was due to the discretization scheme that organically relates the physical behavior to the mathematics. The proposed FVM has twofold character, one in the time and other in the space discretizations. We have applied the new third order algorithm for time discretization of the governing equations. This method resulted in the rapid convergence in comparison to the fourth-order Runge-Kutta scheme [I7]. For the space discretization, the information of the neighbouring cells for finding the flow parameters at corners has been used. Then by using Taylor's expansion, we calculate the values of the first-order derivatives. In this way, the discretization of the viscous and thermal conduction terms are very simplified as similar to the Jameson's flux averaging for the convective terms, while for viscous and thermal conduction terms, the first-order derivatives are averaged in the vicinity of two cells. The proposed FVM is able to converge at higher Reynolds numbers up to 101000. The choice of the cell arrangement for the evaluation of first and second-order derivatives is crucial for the suppression of odd-even decoupling. In the proposed FVM the convective and viscous terms were treated using a novel approach, which in turn resulted in the widened stability range. An attractive feature of the proposed FVM is its capability for vector processing.

8. NOMENCLATURE

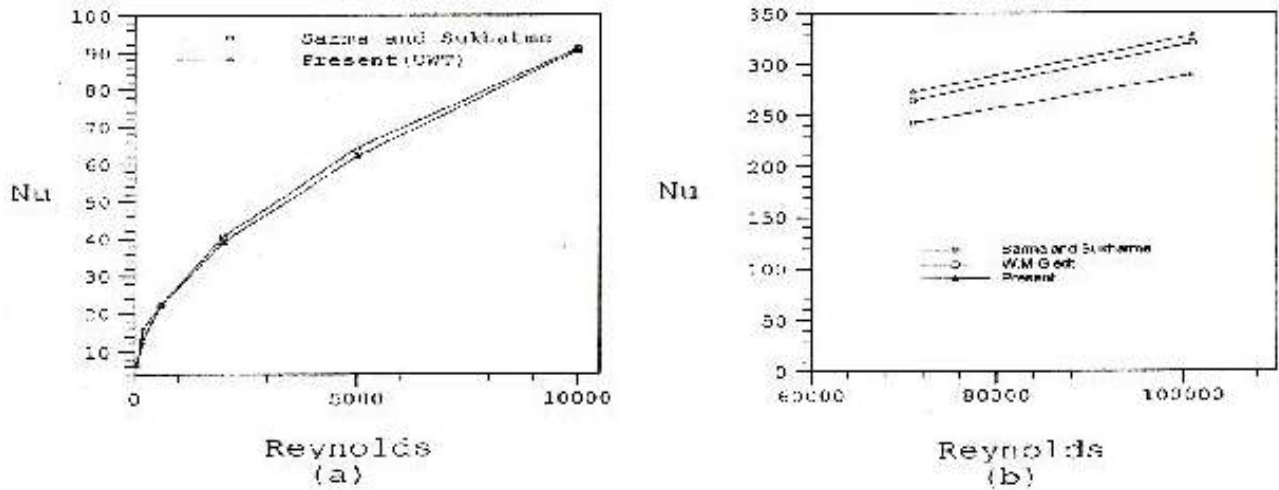|	
A	Cell area
C_D	Drag coefficient
D	Diameter
Error	Residual
IM	Maximum number of circumferential cells
JM	Maximum number of radial cells

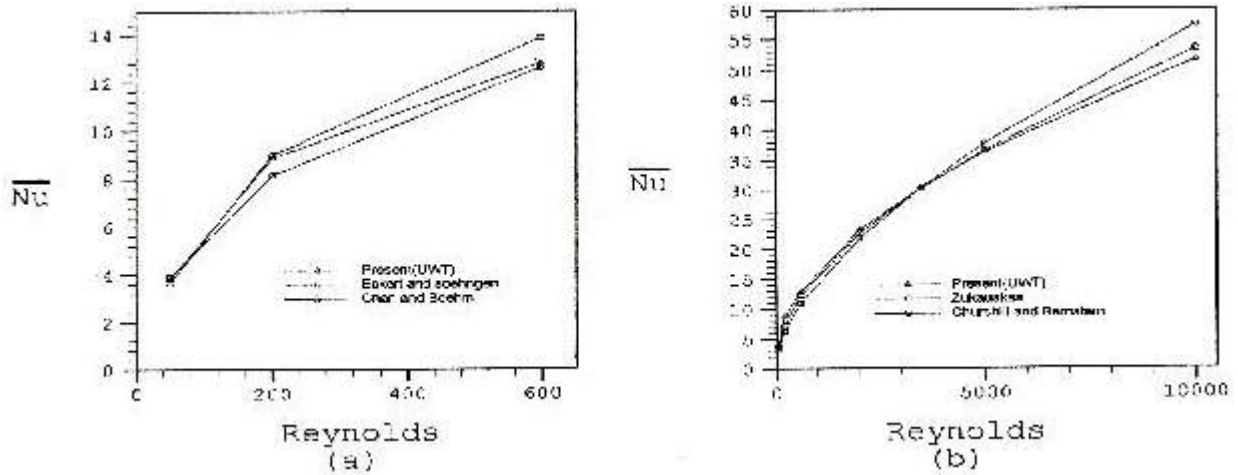**Figure 11**. The peak values of the Nu at the front of stagnation point.

Figure 12. Comparison of average Nusselt numbers with: a)The other numerical solutions, b)The other experimental data.

		Greek	
L	Aigenvector		
Nu	Local Nusselt number	α	Thermal diffusivity
$\overline{Nu}$	Average Nusselt number	β	Artificial compressibility parameter
p	Pressure	ν	Kinematic viscosity
Pr	Prandtl number	η	Clustring parameter
Re	Reynolds number	∂A	Perimeter
u	Velocity along x direction	Δt	Time step
UWT	Uniform wall temperature	θ	Temperature
v	Velocity along y direction		

Superscripts

-               Mean
n   Time level

Subscripts

∞ Free-stream
i   Number of circumferential cells
j   Number of radial cells
m   Mean

9. REFERENCES

1. Zukauskas, A. and Ziugzda, J., "Heat Transfer of a Cylinder in Cross Flow", Hemisphere. Pub. Co., (1985).
2. Schlichting, H., "Boundary-Layer Theory", McGraw. Hill, Inc., (1968).
3. Krall, K. M. and Eckert, E. R. G., "Heat Transfer to a Transverse Circular at Low Raynolds Numbers Including Rarefaction Effects", *Heat Transfer*, Vol. 3, Elsevier, Amsterdam, The Netherlands, (1970), 225-232.
4. Chun, W. and Boehm, R. F., "Calculation of Forced Flow and Heat Transfer - Around a Cylinder in Cross Flow", *Numerical Heat Transfer*, Vol. 15, (1989), 101-122.
5. Anderson, D. A., "Computational Fluid Mechanics and Heat Transfer", Hemisphere Pub. Co., (1984).
6. Kallinderis, J. G., "The Finite Volume Approach for the Navier-Stokes Equations", Computational Meth. in Viscous Aerodynamics, Ed. by Murthy T. K. S. and Brebbia C. A., (1990), 117-144.
7. Jameson, A., Schmidt, W. and Turkel, E., "Numerical Solution of the Euler Equations by Finite Volume Methods Using Runge-Kutta Time Stepping Schems", *AIAA, 14th Fluid and Plasma Dynamics Conf.*, (1981), 81-1259.
8. Jameson, A., Mavriplis, D., "Finite Volume Solution of the Two-Dimensional Euler Equations on a Regular Triangular Mesh", *AIAA J.*, Vol.24, No.4, (1986), 611-618.
9. Pan, D. and Cheng, J. C., "Upwind Finite-Volume Navier-Stokes Computations on Unstructured Triangular Meshes", *AIAA J.*, Vol. 31, No. 9, (1993).
10. Razavy, S. E. and Mateescu, D., "Far-Field Boundary Conditions for Internal Compressible Flows", *Eleventh Canadian Symposium on Fluid Dynamics*, Alberta, Canada, (1994).
11. Dartzi, P. and Cheng, J. C., "Upwind Finite-Volume Navier-Stokes Computations on Unstructured Triangular Meshes", *AIAA J.*, Vol. 31, No. 9, (1993).
12. Yang, S. L. and Chang, Y. L., "Navier-Stokes Computation of the NREL Airfoil Using $K - \omega$ Turbulent Model at High Angles of Attack", *Trans. of ASME*, Vol. 1 17, (1995), 304.
13. Kallinderis, Y., "A Finite Volume Navier-Stokes Algorithm for Adaptive Grids", *In. J. for Num. Meth. in Fluids*, Vol. 15, (1992), 193-217.
14. Razavi, S. E. and Mirzaee, B., "An Enhanced Finite-Volume Method for Computation of Compressible External Flows", *3rd International ISME Conf*, Tehran, (1998).
15. Lin, S. Y. and Wu, T. M., "An Adaptive Multigrid Finite-Volume Scheme for Incompressible Navier-Stokes Equations", *Int. J. for Num. Meth. in Fluids*, Vol. 17, (1993), 683-710.
16. Razavi, S. E. and Mirzaee, B., "An Enhanced Lax-Wendroff Scheme for Solving the Compressible Flows in All Regimes", *5th ISME Conf*, Tabriz, Iran, (1997).
17. Mirzaee, B., "Finite Volume Solution of a Cylinder in Cross Flow with Heat Transfer", Ph.D. Thesis, University of Tabriz, (2001).
18. Incropera, E. P. and Dewitt, D. P., "Introduction to Heat Transfer", John Wiley and Sons, (1990).